

A Transfer Attack to Image Watermarks

Yuepeng Hu, Zhengyuan Jiang, Moyang Guo, Neil Gong
Duke University

{yuepeng.hu, zhengyuan.jiang, moyang.guo, neil.gong}@duke.edu

Abstract

Watermark has been widely deployed by industry to detect AI-generated images. The robustness of such watermark-based detector against evasion attacks in the white-box and black-box settings is well understood in the literature. However, the robustness in the *no-box* setting is much less understood. In particular, multiple studies claimed that image watermark is robust in such setting. In this work, we propose a new transfer evasion attack to image watermark in the no-box setting. Our transfer attack adds a perturbation to a watermarked image to evade multiple surrogate watermarking models trained by the attacker itself, and the perturbed watermarked image also evades the target watermarking model. Our major contribution is to show that, both *theoretically* and *empirically*, watermark-based AI-generated image detector is not robust to evasion attacks even if the attacker does not have access to the watermarking model nor the detection API.

1 Introduction

Generative AI (GenAI) can synthesize extremely realistic-looking images, posing growing challenges to information authenticity on the Internet. Watermarking [1–7] was suggested as a key technology to distinguish AI-generated and non-AI-generated content in the Executive Order on AI security issued by the White House in October 2023. In watermark-based detection, a watermark is embedded into an AI-generated image before releasing it; and an image is detected as AI-generated if the same watermark can be decoded from it. Watermarking AI-generated images has been widely deployed in industry. For instance, Google’s SynthID watermarks images generated by Imagen [8]; OpenAI embeds a watermark into images generated by DALL-E [9]; and Stable Diffusion enables users to embed a watermark into the generated images [10].

An attacker can use *evasion attacks* [11] to remove the watermark in a watermarked image to evade detection. Specifically, an evasion attack strategically adds a perturbation into a watermarked image such that the target watermark-based detector falsely detects the perturbed image as non-AI-generated. The literature has well understood the robustness of watermark-based detector against evasion attacks in the *white-box setting* (i.e., the attacker has access to the target watermarking model) and *black-box setting* (i.e., the attacker has access to the detection API) [11]. Specifically, in the white-box setting, an attacker can find a small perturbation for a given watermarked image such that the perturbed image evades detection while maintaining the image’s visual quality; and in the

black-box setting, an attacker can find such a perturbation once the attacker can query the detection API for enough times.

However, robustness of watermark-based detection in the *no-box setting* (i.e., the attacker does not even have access to the detection API) is much less understood. In such setting, an attacker can use *transfer evasion attacks* (or *transfer attacks* for simplicity) [11, 12]. One transfer attack [11] trains one *surrogate watermarking model* and uses the white-box attack [11] to generate a perturbation for a given watermarked image based on it. An et al. [12], which is *concurrent* to our work, treat a watermark-based detector as a conventional classifier and propose *classifier-based transfer attacks*. For instance, given a set of watermarked and non-watermarked images, an attacker can train a surrogate classifier to distinguish them. Given a watermarked image, the attacker uses conventional adversarial example technique [13] to perturb it such that the surrogate classifier predicts the perturbed image as non-watermarked. Prior studies [11, 12] found that existing transfer attacks have limited success at evading advanced watermarking methods [2, 3]. Thus, a common conclusion in prior studies is that watermarking is robust in the no-box setting.

Our work: In this work, we propose a new transfer attack in the no-box setting to evade watermark-based detection of AI-generated images. Unlike classifier-based transfer attacks [12], our attack directly leverages surrogate watermarking models and thus is better tailored to watermark-based detection. Specifically, an attacker trains multiple surrogate watermarking models using a *surrogate dataset*. The surrogate watermarking models may have different neural network architectures and watermark lengths, compared to the target watermarking model; and the surrogate dataset may have a different distribution from the one used to train the target watermarking model.

Given multiple surrogate watermarking models, a key challenge is how to find a small perturbation for a given watermarked image such that the perturbed image evades the target watermarking model. We propose a two-step approach to address the challenge. In the first step, the attacker picks a watermark (called *target watermark*) for each surrogate watermarking model to guide the perturbation search process. Specifically, the perturbation aims to make each surrogate watermarking model decode the target watermark from the perturbed image. For instance, one way is to flip each bit of the watermark decoded by a surrogate watermarking model for the watermarked image and treat the flipped watermark as the corresponding target watermark. Our intuition is that if the perturbation makes multiple surrogate watermarking models decode flipped watermarks from the perturbed image, the target watermarking model is also likely to decode a flipped watermark from the perturbed image, evading detection.

In the second step, given the target watermark for each surrogate watermarking model, we generate a perturbation by aggregating multiple surrogate watermarking models. For instance, one way is to leverage an existing white-box attack [11] to find a perturbation based on each surrogate watermarking model and its target watermark; and then aggregate the multiple perturbations (e.g., take their mean) as the final perturbation. However, such strategy achieves limited success because the aggregation breaks the perturbation patterns, as shown in our experiments. To address the challenge, we find a perturbation by ensembling multiple surrogate watermarking models. Specifically, we formulate an optimization problem, whose objective function is to find a minimum perturbation and constraints are that each surrogate watermarking model decodes its target watermark from the perturbed image. However, the optimization problem is challenging to solve due to the hard constraints. We propose several strategies to reformulate the optimization

problem and approximately solve it to find a perturbation.

We theoretically analyze the transferability of our transfer attack. Specifically, we formally quantify the correlation between the target and surrogate watermarking models. Based on such quantified correlation, we derive the probability that the watermark decoded by the target watermarking model from the watermarked image is flipped after adding the perturbation found by our transfer attack to it. Moreover, based on this probability, we further derive both an upper bound and a lower bound for the probability that the watermark decoded by the target watermarking model from the perturbed image matches with the ground-truth watermark in the watermarked image. Such upper and lower bounds quantify the transferability of our attack.

We empirically evaluate our transfer attack on image datasets generated by two GenAI models, i.e., Stable Diffusion and Midjourney. We use HiDDeN [2], which is the state-of-art image watermarking method. Our results show that, with dozens of surrogate watermarking models, our attack successfully evades a watermark-based detector while maintaining image quality, even if the surrogate watermarking models use different neural network architectures and watermark lengths from the target one, and are trained using datasets with different distributions. Moreover, our attack substantially outperforms existing transfer attacks [11, 12]. Our results invalidate the prior beliefs that image watermarks are robust in the no-box setting.

To summarize, our contributions are as follows:

- We propose a new transfer attack based on multiple surrogate watermarking models to watermark-based AI-generated image detector.
- We theoretically analyze the effectiveness of our attack.
- We empirically evaluate our transfer attack and compare it with existing ones in different scenarios.

2 Related Work

2.1 Image Watermarks

Three components: An image watermarking method consists of three components: a *watermark* that is a bitstring, an *encoder* that embeds a watermark into an image, and a *decoder* that decodes a watermark from an image. In *non-learning-based methods* [1, 5, 14–16] that have been studied for decades, the encoder and decoder are handcrafted. Unlike these traditional, non-learning-based methods, *learning-based methods* [2–4] leverage deep learning. In these methods, both the encoder and decoder are neural networks and trained in an end-to-end manner using an image dataset. The encoder transforms a watermark and an image into feature vectors and combines them to generate a watermarked image; while the decoder outputs a watermark when taking an (unwatermarked or watermarked) image as input. When jointly training the encoder and decoder, the objectives are to minimize the visual difference between an image and its watermarked version while ensuring accurate decoding of the watermark. Compared to non-learning-based ones, learning-based methods are more robust because they can leverage adversarial training [2]. Therefore, we focus on learning-based methods.

Adversarial training: Adversarial training [13, 17] is a standard method to train robust classifiers and has been extended to train robust watermarking models [2]. The key idea is to add a *post-processing layer* between the encoder and decoder. The post-processing layer aims to mimic post-processing that a watermarked image may undergo in practice. Specifically, the post-processing layer post-processes a watermarked image before sending it to the decoder. After jointly training the encoder and decoder using adversarial training, the decoder can still decode the watermark in a watermarked image even if it undergoes some post-processing. Thus, we use adversarial training in our experiments to train encoders and decoders.

2.2 Evasion Attacks

White-box: Jiang et al. [11] proposed a white-box attack which assumes the attacker has access to the target watermark decoder. Given the target watermark decoder and a watermarked image, an attacker finds a small perturbation such that the watermark decoded from the perturbed image is close to a random watermark. In other words, the perturbation removes the watermark from the watermarked image and thus the perturbed image evades watermark-based detection. Specifically, the attacker finds the perturbation by solving an optimization problem via gradient descent.

Black-box: In black-box setting, an attacker has access to the API of a target watermark-based detector. Given an image, the detection API returns a binary classification result, i.e., AI-generated (watermarked) or non-AI-generated (non-watermarked). A black-box attack [11] leverages the detection API to perturb a watermarked image to remove its watermark. In particular, given a watermarked image, the attacker starts from an initial perturbed image that is detected as non-AI-generated by the API. The initial perturbed image may have a large perturbation compared to the watermarked image. Then, the attacker repeatedly queries the API and gradually moves the perturbed image towards the watermarked image to reduce the perturbation based on the query results. When an attacker can query the API for enough times, the attacker can find a perturbed image with a small perturbation that evades detection of the API.

No-box: In this setting, an attacker does not even have access to the detection API. In such setting, *common post-processing* or *transfer attacks* can be used to remove watermark from a watermarked image. Specifically, common post-processing refers to common image editing operations such as JPEG compression, Gaussian noise, and Gaussian blur. Watermarks embedded by non-learning-based methods can be removed by common post-processing, but learning-based methods have good robustness against common post-processing due to adversarial training [2]. Existing transfer attacks leverage either only one surrogate watermarking model [11] or classifier-based attacks [12] (these attacks are concurrent to ours). For instance, Jiang et al. [11] proposed to train one surrogate encoder and decoder, and then apply the white-box attack [11] to find a perturbation for a given watermarked image based on the surrogate decoder. An example of classifier-based transfer attack [12] is to train a classifier that distinguishes between watermarked and non-watermarked images; and given a watermarked image, the attacker finds a perturbation such that the perturbed image is classified as non-watermarked by the classifier. As shown in prior works [11, 12] and also confirmed in our experiments, these transfer attacks achieve limited success at evading learning-based watermarking methods.

2.3 Transfer Adversarial Examples

Ensemble-based transfer adversarial examples by leveraging multiple surrogate models have been explored within the adversarial examples community [18, 19]. However, these studies focused on ensemble-based transfer attacks to classifiers, where the surrogate and target models are classifiers. Classifiers are qualitatively different from watermarking decoders. Specifically, a classifier outputs a label for an input, while a watermarking decoder outputs a binary string comprising multiple bits. Such difference results in a fundamentally different optimization objective for transfer attacks. Furthermore, the binary nature of watermark bitstrings enables us to carry out rigorous theoretical analysis on the effectiveness of our transfer attack. However, it is challenging to conduct such theoretical analysis for transfer attacks to classifiers.

3 Problem Formulation

3.1 Watermark-Based Detection

A GenAI service provider trains a watermark encoder (called *target encoder*) and decoder (called *target decoder* and denoted as T), and uses them for AI-generated image detection. During generation, a watermark w is embedded into each AI-generated image using the target encoder. During detection, a watermark is decoded from a given image x by the target decoder T . We denote by $T(x)$ the decoded watermark. We represent the *bitwise accuracy* between two watermarks w_1 and w_2 as $BA(w_1, w_2)$, which is the proportion of bits that are identical in w_1 and w_2 . Watermark-based detection determines whether the image x is AI-generated based on the bitwise accuracy $BA(T(x), w)$ between the decoded watermark $T(x)$ and the ground-truth watermark w . Specifically, the image x is detected as AI-generated if the bitwise accuracy $BA(T(x), w)$ either exceeds a certain threshold τ or falls below $1 - \tau$, i.e., $BA(T(x), w) > \tau$ or $BA(T(x), w) < 1 - \tau$. τ is commonly set to a value such that the false detection rate, i.e., the probability of falsely detecting a non-AI-generated (i.e., non-watermarked) image as AI-generated (i.e., watermarked), does not exceed a desired small value η [11]. For instance, when the watermark has 30 bits and $\eta = 10^{-4}$, $\tau \approx 0.83$.

The detector discussed above is known as *double-tail detector* [11]. In a *single-tail detector*, the image x is detected as AI-generated if the bitwise accuracy $BA(T(x), w)$ exceeds a threshold τ , i.e., $BA(T(x), w) > \tau$. Double-tail detector is more robust than single-tail detector, e.g., if a perturbed watermarked image evades double-tail detector, then it also evades single-tail detector, but not vice versa. Therefore, we focus on double-tail detector in this work.

3.2 Threat Model

Attacker’s goal: Suppose an attacker uses a GenAI service to produce a watermarked image x_w . The attacker’s goal is to introduce a minimal perturbation δ to the watermarked image x_w , aiming to evade watermark-based detection while preserving image quality. Consequently, the attacker can engage in illicit activities using this image, such as boosting disinformation and propaganda campaigns as well as claiming ownership of the image.

Attacker’s knowledge: A GenAI service provider’s watermark-based detector includes a target encoder, a target decoder, a ground-truth watermark w , and a detection threshold τ . We assume that the attacker has *no-box* access to the watermark-based detector. Specifically, the attacker does not have access to the target encoder, target decoder, ground-truth watermark w , and detection threshold τ . Moreover, the attacker does not know the neural network architecture of the target encoder and decoder, the length of the ground-truth watermark w , nor the image dataset used to train the target encoder/decoder. Such threat model arises when the GenAI service sets its watermark-based detector private and restricts access of the detection API to trusted customers.

Attacker’s capability: We assume an attacker can add a perturbation to an AI-generated, watermarked image. Furthermore, we assume that the attacker has sufficient computational resources to train multiple surrogate watermarking models, where each surrogate watermarking model includes a surrogate encoder and a surrogate decoder.

4 Our Transfer Attack

4.1 Overview

We propose a transfer attack to evade watermark-based AI-generated image detection. Our transfer attack trains multiple surrogate watermarking models, and then generates a perturbation for a given watermarked image based on them. We train a set of diverse surrogate watermarking models independently using a dataset that may have a different distribution from the one used by the target watermarking model. For a given watermarked image x_w , we generate a perturbation δ based on the surrogate decoders such that the watermark decoded by each surrogate decoder for the perturbed image $x_w + \delta$ substantially differs from the watermark decoded for the original watermarked image x_w . Our intuition is that if multiple surrogate decoders decode a substantially different watermark for the perturbed image $x_w + \delta$, it is likely that the target watermarking decoder would decode a substantially different watermark, evading detection. Note that the same surrogate decoders are used to generate perturbations for all watermarked images.

Next, we describe the details of training surrogate models and generating perturbations based on them.

4.2 Train Surrogate Watermarking Models

Transfer attacks require a set of surrogate watermarking models to produce perturbation for a watermarked image. To improve the transferability of the perturbation produced in our transfer attack, a crucial challenge is to encourage diversity among the surrogate watermarking models. The attacker first collects an image dataset (called *surrogate dataset*) to train the surrogate watermarking models. The surrogate dataset may have a different distribution from the dataset used to train the target watermarking model. To encourage diversity, we propose to adopt *bootstrapping* [20], which is a widely used technique to train diverse models in statistics. Specifically, the attacker resamples m subsets from the surrogate dataset, each of which is used to train one of the m surrogate watermarking models. Moreover, the attacker can use different neural network architectures and different watermark lengths for the m surrogate watermarking models.

4.3 Formulate an Optimization Problem

To evade watermark-based detection, we generate a perturbation δ for a given watermarked image x_w based on the m surrogate decoders since the detection process only involves decoders. Specifically, our goal is to add a perturbation δ to the watermarked image x_w such that, for each surrogate decoder, the decoded watermark from the perturbed image $x_w + \delta$ matches an attacker-chosen watermark, which we call *target watermark*. Our transfer attack faces two key challenges: 1) how to select a target watermark for a surrogate decoder, and 2) how to generate a perturbation δ based on the m target watermarks and surrogate decoders. We discuss how to address the two challenges in the following.

Select a target watermark for a surrogate decoder: We use w_i^t to denote the target watermark for the i th surrogate decoder, where $i = 1, 2, \dots, m$. We consider the following approaches to select w_i^t .

Random-Different (RD). This method involves randomly generating different target watermarks for the m surrogate decoders. For the i th surrogate decoder, each bit of w_i^t is sampled from $\{0, 1\}$ uniformly at random. The intuition of this method is that, if the m surrogate decoders decode random watermarks from the perturbed image, then the target decoder is also likely to decode a random watermark from the perturbed image. As a result, the bitwise accuracy between the watermark $T(x_w + \delta)$ decoded by the target decoder for the perturbed image and the ground-truth watermark w is expected to approach 0.5, thereby evading detection.

Random-Same (RS). This method randomly generates one random target watermark w^t for all m surrogate decoders, i.e., $w_i^t = w^t, \forall i = 1, 2, \dots, m$. The intuition is that it is more likely to find a perturbation δ such that the m surrogate decoders decode the same target watermark from the perturbed image, and thus it is more likely for the target decoder to decode w^t from the perturbed image. Since w^t is picked uniformly at random, the bitwise accuracy between w^t and w is expected to approach 0.5 and detection is evaded.

Inverse-Decode (ID). However, generating random watermarks as target watermarks for surrogate decoders may have an issue. Specifically, for each surrogate decoder, approximately 50% of the bits require to be flipped while optimizing the perturbation, given that each bit of the target watermark is uniformly sampled from $\{0, 1\}$. Among these bits to be flipped, some may be very robust to pixel changes and thus large perturbation is required to alter them.

To address this issue, we propose to use the inverse of the watermark decoded by each surrogate decoder as the corresponding target watermark. Specifically, we use S_i to denote the i th surrogate decoder. For a watermarked image x_w , S_i decodes a watermark from it, denoted as $S_i(x_w)$. We use the inverse of the decoded watermark, i.e., $1 - S_i(x_w)$, as the target watermark w_i^t for the i th surrogate decoder S_i , where $1 - S_i(x_w)$ means flipping each bit of $S_i(x_w)$. The intuition of this method is that the watermark decoded by each surrogate decoder from the perturbed image is reversed, and thus it is likely that the watermark decoded by the target decoder from the perturbed image is also reversed, i.e., $T(x_w + \delta)$ is close to $1 - T(x_w)$. As a result, the bitwise accuracy between $T(x_w + \delta)$ and w is very small since $T(x_w)$ is close to w . We note that such bitwise accuracy may be even smaller than $1 - \tau$, which means that the double-tail detector can still detect the perturbed image as AI-generated, watermarked image. We address this challenge by

early stopping the process of finding the perturbation δ , which we discuss in Section 4.4.

With the inverse watermark as target watermark, it may result in those bits that are less robust to pixel changes being flipped first during perturbation optimization process. As a result, it can lead to a smaller perturbation compared to random target watermark when the same portion of bits are flipped, as shown in our experiments.

Aggregate m surrogate decoders: Given a target watermark w_i^t for the i th surrogate decoder, the attacker then finds a perturbation δ for the watermarked image x_w by aggregating the m surrogate decoders. We consider the following two ways to aggregate the m surrogate decoders.

Post-Aggregate (PA). A straightforward way is to apply an existing white-box attack to find a perturbation δ_i based on the i th surrogate decoder and target watermark. For instance, given the watermarked image x_w , i th surrogate decoder S_i , and target watermark w_i^t , the attacker can use the state-of-the-art white-box attack in Jiang et al. [11] to find the perturbation δ_i . Formally, the attacker gets m perturbations $\{\delta_i\}_{i=1}^m$. Then, the attacker can aggregate them as the final perturbation δ , i.e., $\delta = \text{aggr}(\delta_1, \dots, \delta_m)$, where aggr is an aggregation method. For instance, aggr can be *Mean* or *Median*, which takes the mean or median of the m perturbations as the final perturbation δ . However, aggregating the perturbations generated by the surrogate decoders may ruin the patterns in them which are effective to mislead the target decoder before aggregation. As a result, the obtained perturbation achieves limited transferability to the target decoder, as shown in our experiments.

Ensemble-Optimization (EO). To address the challenge of Post-Aggregate, Ensemble-Optimization considers the m surrogate decoders when optimizing the perturbation δ . Specifically, Ensemble-Optimization aims to find a minimum perturbation such that the watermark $S_i(x_w + \delta)$ decoded by each surrogate decoder for the perturbed image $x_w + \delta$ is the same as its corresponding target watermark w_i^t . Formally, we formulate an optimization problem as follows:

$$\begin{aligned} \min_{\delta} \quad & \|\delta\|_{\infty} \\ \text{s.t.} \quad & S_i(x_w + \delta) = w_i^t, \forall i = 1, 2, \dots, m \end{aligned} \tag{1}$$

Ensemble-Optimization finds a shared perturbation δ such that all the m surrogate decoders output their target watermarks for the perturbed image $x_w + \delta$. The generalization ability of the shared perturbation for all surrogate decoders could enhance the transferability to the target decoder, as shown in our experiments. Note that we use ℓ_{∞} -norm to measure the magnitude of the perturbation. Our method is also applicable to other metrics such as ℓ_2 or SSIM, as shown in our experiments.

4.4 Solve the Optimization Problem

Solving the optimization problem in Equation 1 gets the perturbation δ for the watermarked image x_w . However, since the constraints of the optimization problem are extremely strict, it is difficult to solve the optimization problem. To address this challenge, we relax the constraints and reformulate the optimization problem as follows:

$$\begin{aligned} \min_{\delta} \quad & \|\delta\|_{\infty} \\ \text{s.t.} \quad & l(S_i(x_w + \delta), w_i^t) < \epsilon, \forall i = 1, 2, \dots, m, \end{aligned} \tag{2}$$

where $l(\cdot, \cdot)$ denotes a metric to measure the distance between two watermarks. For instance, $l(\cdot, \cdot)$ is the mean square error in our experiments.

The reformulated optimization problem is still challenging to solve due to the high non-linearity of the relaxed constraints. To address this challenge, we further reformulate the optimization problem as follows:

$$\begin{aligned} \min_{\delta} \quad & \frac{1}{m} \sum_{i=1}^m l(S_i(x_w + \delta), w_i^t) \\ \text{s.t.} \quad & \|\delta\|_{\infty} < r, \\ & \frac{1}{m} \sum_{i=1}^m BA(S_i(x_w + \delta), w_i^t) > 1 - \epsilon, \end{aligned} \tag{3}$$

where r is a perturbation budget and ϵ (called *attack strength threshold*) is used to ensure that the bitwise accuracy between the watermark decoded by each surrogate decoder for the perturbed image and the corresponding target watermark is high enough to produce an effective perturbation.

We use projected gradient descent (PGD) [13] to solve the optimization problem in Equation 3. To better control the strength of our transfer attack to evade double-tail detector, we consider the second constraint in the optimization problem in Equation 3 as a condition for early stopping. Our detailed algorithm to find the perturbation δ is shown in Algorithm 1 in Appendix. It first initializes δ to zero and then compute the gradient of the objective function as defined in Equation 3 with respect to δ . The gradient is then used to update δ according to gradient descend. If the ℓ_{∞} -norm of the updated δ exceeds r , it is then projected onto the ℓ_{∞} -norm ball with radius r . The algorithm terminates and outputs the final perturbation δ once the number of optimization iterations or the average bitwise accuracy exceeds a predefined threshold.

5 Theoretical Analysis

We conduct theoretical analysis about the transferability of our transfer attack. Specifically, given the watermarks decoded by the m surrogate decoders for the perturbed image, we derive both an upper bound and a lower bound for the probability that the watermark decoded by the target decoder for the perturbed image matches with the ground-truth watermark. All our proofs are shown in Appendix.

5.1 Notations

We adopt T to denote the target decoder and $\{S_i\}_{i=1}^m$ to represent the m surrogate decoders. w denotes the ground-truth watermark and x_w denotes a watermarked image embedded with w . δ denotes a perturbation that satisfies the constraints of the optimization problem in Equation 3. For simplicity, we assume the target decoder and surrogate decoders use the same watermark length, which we denote as n . $T(\cdot)_j$ and $S_i(\cdot)_j$ denote the j th bit of the watermarks decoded by T and S_i for an image, respectively. Moreover, we consider inverse watermarks as the target watermarks in our transfer attack.

5.2 Formal Definitions and Assumptions

To analyze the transferability between surrogate decoders and target decoder, we need to formally quantify their relationships. Towards this goal, we define *unperturbed similarity*, *positive transferring similarity*, and *negative transferring similarity*. Unperturbed similarity measures the probability that the watermarks decoded by the target decoder and surrogate decoders are identical for a watermarked image x_w without perturbation, which is formally defined as follows:

Definition 1 (Unperturbed similarity). *For any watermarked image x_w and δ satisfying the constraints of the optimization problem in Equation 3, the j th bit of the watermark decoded by T matches with the j th bit of the watermark decoded by S_i for x_w with probability k_{ij} , given that the j th bits of the watermarks for $x_w + \delta$ and x_w decoded by S_i are inverse. Conversely, it occurs with probability k'_{ij} given that the j th bits of the watermarks for $x_w + \delta$ and x_w decoded by S_i are identical. Formally, for $i = 1, 2, \dots, m$ and $j = 1, 2, \dots, n$, we have:*

$$\begin{aligned} Pr(T(x_w)_j = S_i(x_w)_j \mid S_i(x_w + \delta)_j = 1 - S_i(x_w)_j) &= k_{ij}, \\ Pr(T(x_w)_j = S_i(x_w)_j \mid S_i(x_w + \delta)_j = S_i(x_w)_j) &= k'_{ij}. \end{aligned} \quad (4)$$

Note that both k_{ij} and k'_{ij} can be estimated in experiments. Positive transferring similarity measures the probability that the watermarks decoded by target decoder and surrogate decoders for a perturbed image $x_w + \delta$ are identical when the watermarks decoded by the surrogate decoders are flipped after adding the perturbation, which is defined as follows:

Definition 2 (Positive transferring similarity). *For any watermarked image x_w and δ satisfying the constraints of the optimization problem in Equation 3, the j th bit of the watermark decoded by T matches with the j th bit of the watermark decoded by S_i for $x_w + \delta$ with probability a_{ij} , given that the j th bits of the watermarks decoded by T and S_i are identical for x_w , and the j th bits of the watermarks for $x_w + \delta$ and x_w decoded by S_i are inverse. Conversely, it occurs with probability a'_{ij} given that the j th bits of the watermarks decoded by T and S_i for x_w are inverse, and the j th bits of the watermarks for $x_w + \delta$ and x_w decoded by S_i are also inverse. Formally, for $i = 1, 2, \dots, m$ and $j = 1, 2, \dots, n$, we have the following:*

$$\begin{aligned} Pr(T(x_w + \delta)_j = S_i(x_w + \delta)_j \mid T(x_w)_j = S_i(x_w)_j, \\ S_i(x_w + \delta)_j = 1 - S_i(x_w)_j) &= a_{ij}, \\ Pr(T(x_w + \delta)_j = S_i(x_w + \delta)_j \mid T(x_w)_j = 1 - S_i(x_w)_j, \\ S_i(x_w + \delta)_j = 1 - S_i(x_w)_j) &= a'_{ij}. \end{aligned} \quad (5)$$

Both a_{ij} and a'_{ij} can be estimated in experiments. Similarly, we use negative transferring similarity to measure the probability that the watermarks decoded by target decoder and surrogate decoders for a perturbed image $x_w + \delta$ are identical when the outputs of surrogate decoders remain unchanged after adding the perturbation, which is defined as follows:

Definition 3 (Negative transferring similarity). *For any watermarked image x_w and δ satisfying the constraints of the optimization problem in Equation 3, the j th bit of the watermark decoded by T matches with the j th bit of the watermark decoded by S_i for*

$x_w + \delta$ with probability b_{ij} , given that the j th bits of the watermarks decoded by T and S_i are inverse for x_w , and the j th bits of the watermarks for $x_w + \delta$ and x_w decoded by S_i are identical. Conversely, it occurs with probability b'_{ij} given that the j th bits of the watermarks decoded by T and S_i for x_w are identical, and the j th bits of the watermarks for $x_w + \delta$ and x_w decoded by S_i are also identical. Formally, for $i = 1, 2, \dots, m$ and $j = 1, 2, \dots, n$, we have the following:

$$\begin{aligned} Pr(T(x_w + \delta)_j = S_i(x_w + \delta)_j \mid T(x_w)_j = 1 - S_i(x_w)_j, \\ S_i(x_w + \delta)_j = S_i(x_w)_j) &= b_{ij}, \\ Pr(T(x_w + \delta)_j = S_i(x_w + \delta)_j \mid T(x_w)_j = S_i(x_w)_j, \\ S_i(x_w + \delta)_j = S_i(x_w)_j) &= b'_{ij}. \end{aligned} \tag{6}$$

Both b_{ij} and b'_{ij} can be estimated in experiments. To quantify the magnitude of our transfer attack, we formally define the q -attacking strength which measures the probability that the watermarks for the perturbed image and the watermarked image decoded by surrogate decoders are inverse as follows:

Definition 4 (q -attacking strength). *For any watermarked image x_w and δ satisfying the constraints of the optimization problem in Equation 3, the j th bit of the watermark decoded by S_i for the perturbed image is the inverse of the j th bit of the watermark decoded by S_i for the watermarked image with probability q_{ij} . Formally, we have the following:*

$$Pr(S_i(x_w + \delta)_j = 1 - S_i(x_w)_j) = q_{ij}. \tag{7}$$

q_{ij} can also be estimated in experiments. To quantify the performance of the target watermarking model when no perturbations are added to watermarked images, we introduce the following definition on β -accurate watermarking: assume the bitwise accuracy between the watermark decoded by the target decoder for the watermarked image and the ground-truth watermark following Poisson binomial distribution. Specifically, we have the following assumption:

Definition 5 (β -accurate watermarking). *For any watermarked image x_w , the bits of the watermark decoded by T are mutually independent and the probability that the j th bit of the decoded watermark matches with that of the ground-truth watermark w is β_j , where $1 \leq j \leq n$.*

$\beta_1, \beta_2, \dots, \beta_n$ can be estimated in experiments. Next, we introduce three assumptions regarding the surrogate decoders and the target decoder. For *bit-level dependency*, it is assumed that each bit of the watermark decoded by the target decoder only depends on the corresponding bits of the watermarks decoded by the surrogate decoders. Formally, we have the assumption as follows:

Assumption 1 (Bit-level dependency). *For any watermarked image x_w and δ satisfying the constraints of the optimization problem in Equation 3, each bit of the watermark decoded by T for the perturbed image only depends on the corresponding bits of the watermarks decoded by the surrogate decoders for the perturbed image. Formally, we have the following:*

$$\begin{aligned} Pr(T(x_w + \delta)_j \mid S_1(x_w + \delta), \dots, S_m(x_w + \delta)) \\ = Pr(T(x_w + \delta)_j \mid S_1(x_w + \delta)_j, \dots, S_m(x_w + \delta)_j), \forall j. \end{aligned} \tag{8}$$

Additionally, since all the surrogate decoders are trained independently with different subsets of data, we further assume that the watermarks decoded by the surrogate decoders are independent and conditionally independent given the watermark decoded by the target decoder for the watermarked or perturbed image.

Assumption 2 (Independency). *For any watermarked image x_w and δ satisfying the constraints of the optimization problem in Equation 3, the j th bits of the watermarks decoded by the m surrogate decoders for the perturbed image are independent. Formally, we have the following:*

$$\begin{aligned} & Pr(S_1(x_w + \delta)_j, \dots, S_m(x_w + \delta)_j) \\ & = Pr(S_1(x_w + \delta)_j) \cdots Pr(S_m(x_w + \delta)_j), \forall j. \end{aligned} \quad (9)$$

Assumption 3 (Conditional independency). *For any watermarked image x_w and δ satisfying the constraints of the optimization problem in Equation 3, the j th bits of the watermarks decoded by the m surrogate decoders for $x_w + \delta$ are independent when the j th bit of the watermark decoded by the target decoder for x_w or $x_w + \delta$ is given. Formally, we have:*

$$\begin{aligned} & Pr(S_1(x_w + \delta)_j, \dots, S_m(x_w + \delta)_j \mid T(x_w)_j) \\ & = Pr(S_1(x_w + \delta)_j \mid T(x_w)_j) \cdots \\ & \quad Pr(S_m(x_w + \delta)_j \mid T(x_w)_j), \forall j, \\ & Pr(S_1(x_w + \delta)_j, \dots, S_m(x_w + \delta)_j \mid T(x_w + \delta)_j) \\ & = Pr(S_1(x_w + \delta)_j \mid T(x_w + \delta)_j) \cdots \\ & \quad Pr(S_m(x_w + \delta)_j \mid T(x_w + \delta)_j), \forall j. \end{aligned} \quad (10)$$

5.3 Deriving $Pr(T(x_w + \delta)_j = 1 - T(x_w)_j)$

We first derive the probability that the watermark decoded by the target decoder is flipped after adding the perturbation found by our transfer attack to the watermark image, conditioned on that the watermark decoded by a surrogate decoder is flipped or not after adding the perturbation. Formally, we have the following lemma:

Lemma 1. *For any watermarked image x_w and δ satisfying the constraints of the optimization problem in Equation 3, the j th bit of the watermark decoded by T for $x_w + \delta$ is the inverse of the j th bit of the watermark decoded by T for x_w with probability $a_{ij}k_{ij} + (1 - a'_{ij})(1 - k'_{ij})$, given that the j th bits of the watermarks for the $x_w + \delta$ and x_w decoded by S_i are inverse. Conversely, it occurs with probability $(1 - b'_{ij})k'_{ij} + b_{ij}(1 - k'_{ij})$ given that the j th bits of the watermarks for $x_w + \delta$ and x_w decoded by S_i are identical. Formally, we have:*

$$\begin{aligned} & Pr(T(x_w + \delta)_j = 1 - T(x_w)_j \mid S_i(x_w + \delta)_j = 1 - S_i(x_w)_j) \\ & = c_{ij}, \\ & Pr(T(x_w + \delta)_j = 1 - T(x_w)_j \mid S_i(x_w + \delta)_j = S_i(x_w)_j) \\ & = c'_{ij}, \end{aligned} \quad (11)$$

where $c_{ij} = a_{ij}k_{ij} + (1 - a'_{ij})(1 - k_{ij})$ and $c'_{ij} = (1 - b'_{ij})k'_{ij} + b_{ij}(1 - k'_{ij})$.

Then, we derive the unconditional probability that the watermark decoded by the target decoder is flipped after adding the perturbation to the watermarked image as follows:

Theorem 1. For any watermarked image x_w and δ satisfying the constraints of the optimization problem in Equation 3, the j th bit of the watermark decoded by T for the perturbed image is the inverse of the j th bit of the watermark decoded by T for the watermarked image with probability $c_{ij}q_{ij} + c'_{ij}(1 - q_{ij})$. Formally, we have the following:

$$\Pr(T(x_w + \delta)_j = 1 - T(x_w)_j) = e_j, \quad (12)$$

where $e_j = c_{ij}q_{ij} + c'_{ij}(1 - q_{ij}), \forall i$.

Then we derive the probability that the watermarks decoded by the surrogate decoders are flipped when the watermark decoded by the target decoder is flipped after adding the perturbation as follows:

Lemma 2. For any watermarked image x_w and δ satisfying the constraints of the optimization problem in Equation 3, the j th bit of the watermark decoded by S_i for the perturbed image is the inverse of the j th bit of the watermark decoded by S_i for the watermarked image with probability $\frac{c_{ij}q_{ij}}{c_{ij}q_{ij} + c'_{ij}(1 - q_{ij})}$, given that the watermarks for the perturbed image and the watermarked image decoded by T are inverse. Formally, we have the following:

$$\begin{aligned} \Pr(S_i(x_w + \delta)_j = 1 - S_i(x_w)_j \mid T(x_w + \delta)_j = 1 - T(x_w)_j) \\ = \frac{c_{ij}q_{ij}}{c_{ij}q_{ij} + c'_{ij}(1 - q_{ij})}. \end{aligned} \quad (13)$$

Finally, we derive the probability that the watermark decoded by the target decoder is flipped after adding the perturbation to the watermarked image, given the watermarks decoded by the m surrogate decoders for the perturbed image. Formally, we have the following:

Theorem 2. For any watermarked image x_w and δ satisfying the constraints of the optimization problem in Equation 3, the j th bit of the watermark decoded by T for the perturbed image is the inverse of the j th bit of the watermark decoded by T for the watermarked image with probability p_j , when the watermarks for the perturbed image decoded by the m surrogate decoders are given. Formally, we have the following:

$$\begin{aligned} \Pr(T(x_w + \delta)_j = 1 - T(x_w)_j \mid S_1(x_w + \delta)_j, \dots, S_m(x_w + \delta)_j) \\ = p_j, \end{aligned} \quad (14)$$

where $p_j = \min(e_j \prod_{i \in M_{j1}} \frac{c_{ij}}{c_{ij}q_{ij} + c'_{ij}(1 - q_{ij})} \prod_{i \in M_{j2}} \frac{c'_{ij}}{c_{ij}q_{ij} + c'_{ij}(1 - q_{ij})},$

$1)$, $M_{j1} = \{i \mid S_i(x_w + \delta)_j = 1 - S_i(x_w)_j\}$, and $M_{j2} = \{i \mid S_i(x_w + \delta)_j = S_i(x_w)_j\}$. M_{j1} (or M_{j2}) is the set of surrogate decoders whose j th bits of the decoded watermarks flip (or not flip) after adding the perturbation to the watermarked image.

5.4 Deriving $\Pr(T(x_w + \delta)_j = w_j)$

The bitwise accuracy between the decoded watermark $T(x_w + \delta)$ and the ground-truth watermark w is used to detect whether the perturbed image $x_w + \delta$ is AI-generated. Therefore, given the watermarks decoded by the m surrogate decoders for the perturbed image $x_w + \delta$, we derive an upper bound and a lower bound of the probability that the

watermark decoded by the target decoder matches with the ground-truth watermark after adding the perturbation. Formally, based on the theorems in Section 5.3, we further derive the following theorem:

Theorem 3. *Given any watermarked image x_w , δ satisfying the constraints of the optimization problem in Equation 3, and the watermarks decoded by the m surrogate decoders for the perturbed image, we have an upper bound and a lower bound of the probability that the j th bit of the watermark decoded by T for the perturbed image matches with the j th bit of the ground-truth watermark w as follows:*

$$\begin{aligned}
 & Pr(T(x_w + \delta)_j = w_j \mid S_1(x_w + \delta)_j, \dots, S_m(x_w + \delta)_j) \\
 & \geq \max(\beta_j - p_j, 0), \\
 & Pr(T(x_w + \delta)_j = w_j \mid S_1(x_w + \delta)_j, \dots, S_m(x_w + \delta)_j) \\
 & \leq 1 - |p_j + \beta_j - 1|.
 \end{aligned} \tag{15}$$

Such upper bound and lower bound quantify the transferability of our transfer attack. Note that we derive both an upper bound and a lower bound of the probability because we consider double-tail detectors.

6 Experiments

6.1 Experimental setup

Datasets: In our experiments, we utilize AI-generated images for watermarking model training and testing. For the target watermarking models, we use two public datasets [21, 22] generated by Stable Diffusion and Midjourney respectively. Following HiDDeN [2], we randomly select 10,000 images from each dataset to train the target watermarking encoders and decoders. For testing, we randomly sample 1,000 images from the testing set of each dataset, embed the ground-truth watermark into each of them using a target encoder, and then find the perturbation to each watermarked image using different methods. To train the surrogate watermarking models, we sample 10,000 images from another public dataset [23] generated by DALL-E 2, i.e., the surrogate dataset consists of these 10,000 images. The input image size of the watermarking models is 128×128 pixels.

Target and surrogate watermarking model architectures and watermark lengths: For surrogate watermarking models, we employ the convolution neural network architecture described in HiDDeN with the watermark length of 30 bits. We use the same architecture and watermark length for all surrogate watermarking models for two main purposes. Firstly, it can give us a clearer understanding of our attack’s transferability, especially when the target watermarking model and surrogate watermarking models have different architectures and watermark lengths. Secondly, it allows for a better analysis of the impact of the number of surrogate watermarking models on our attack’s transferability, without the confounding effects of variations in architecture and watermark length of the surrogate watermarking models.

For the target watermarking model, we use different choices of architectures and watermark lengths to analyze the transferability of our transfer attack in different scenarios. Specifically, we consider the following architectures for the target watermarking model.

CNN. The target watermarking model has convolution neural network architecture. In particular, the encoder consists of 4 convolutional blocks, while the decoder consists of 7 convolutional blocks. Each block integrates a Convolution layer, Batch Normalization, and ReLU activation.

ResNet. To further evaluate our transfer attack when the target watermarking model’s architecture is more sophisticated than that of the surrogate watermarking models, we also adopt ResNet for the target watermarking model. In particular, the encoder consists of 7 convolutional blocks and the decoder is the ResNet-18.

Additionally, we also employ different watermark lengths for the target watermarking models. Specifically, we evaluate our transfer attack on the target watermarking models with watermark lengths of 20 bits, 30 bits, and 64 bits. These variations include watermark lengths that are shorter than, equal to, and longer than those used by the surrogate watermarking models, offering a thorough analysis of our transfer attack’s performance across different watermark lengths in the target watermarking model.

Common post-processing methods: These methods can be applied in the no-box setting. Therefore, we compare our transfer attack with them. Specifically, we consider the following common post-processing methods.

JPEG. It is a commonly used compression method in digital imaging, which can reduce image file sizes while preserving a reasonable level of image quality. The quality of images processed through JPEG is governed by a quality factor Q . As the quality factor decreases, detecting the watermark in the post-processed images becomes more challenging, although this also results in a lower image quality.

Gaussian noise. This method involves adding statistical noise that follows a Gaussian distribution with a zero mean and a standard deviation of σ , which effectively simulates various environmental noise effects encountered in real-world scenarios. A larger σ value leads to increased difficulty in watermark detection, but also results in lower image quality.

Gaussian blur. This method smooths the image by averaging pixel values with their neighbors. It applies a Gaussian filter with kernel size of $k \times k$ to an image, characterized by a bell-shaped curve with a zero mean and a standard deviation of σ . A larger σ causes more pronounced blurring, which results in lower watermark detection rate and image quality. Following Jiang et al. [11], we set $k = 5$ and vary σ .

Brightness/Contrast. This method modifies the brightness and contrast of an image by adjusting pixel values throughout the image. Specifically, it operates by either increasing or decreasing these values to make the image brighter or darker. The process is regulated by two factors: a brightness factor B and a contrast factor C . Formally, for each pixel value v , the method transforms it to $Cv + B$. Following Jiang et al. [11], we set $B = 0.2$ and vary C .

Transfer attacks: We compare with the following attacks.

WEvade-B-S [11]. This method trains one surrogate watermarking model. During attack, PGD is employed to perturb a watermarked image such that the watermark decoded by the surrogate decoder for the perturbed image matches with a preset randomly generated watermark. In our experiments, we train the surrogate watermarking model on 10,000 images generated by DALL-E 2. To give advantages to this transfer attack, we assume the attacker knows the architecture of the target watermarking model and uses it as the architecture of the surrogate watermarking model.

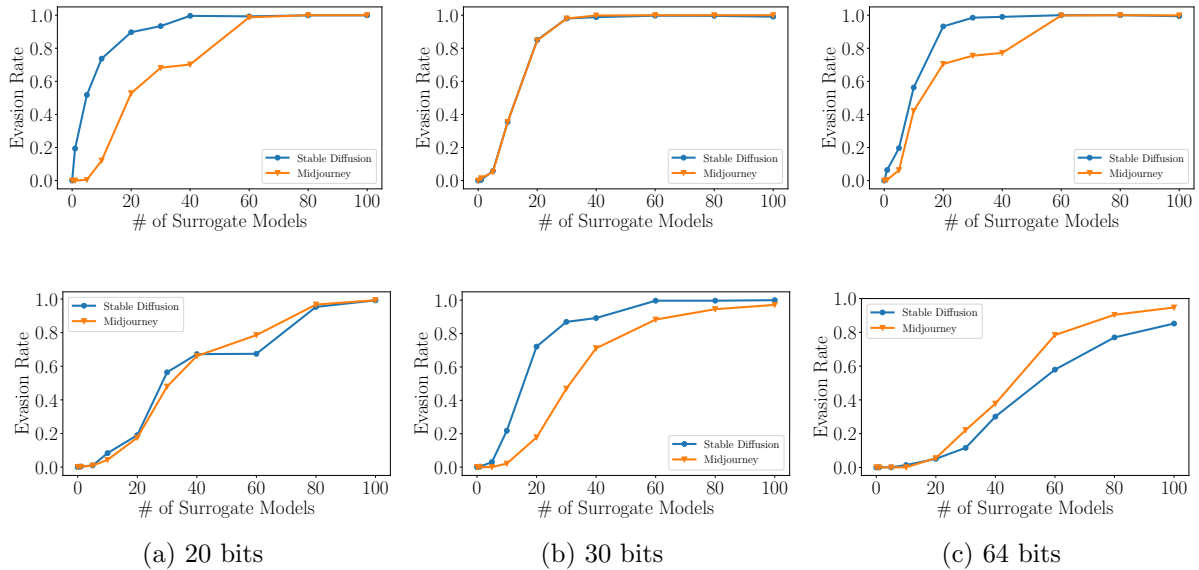


Figure 1: Evasion rate of our transfer attack when the target model uses CNN (*first row*) or ResNet (*second row*) architecture and different watermark lengths (*the three columns*). The surrogate models use CNN architecture and watermark length of 30 bits.

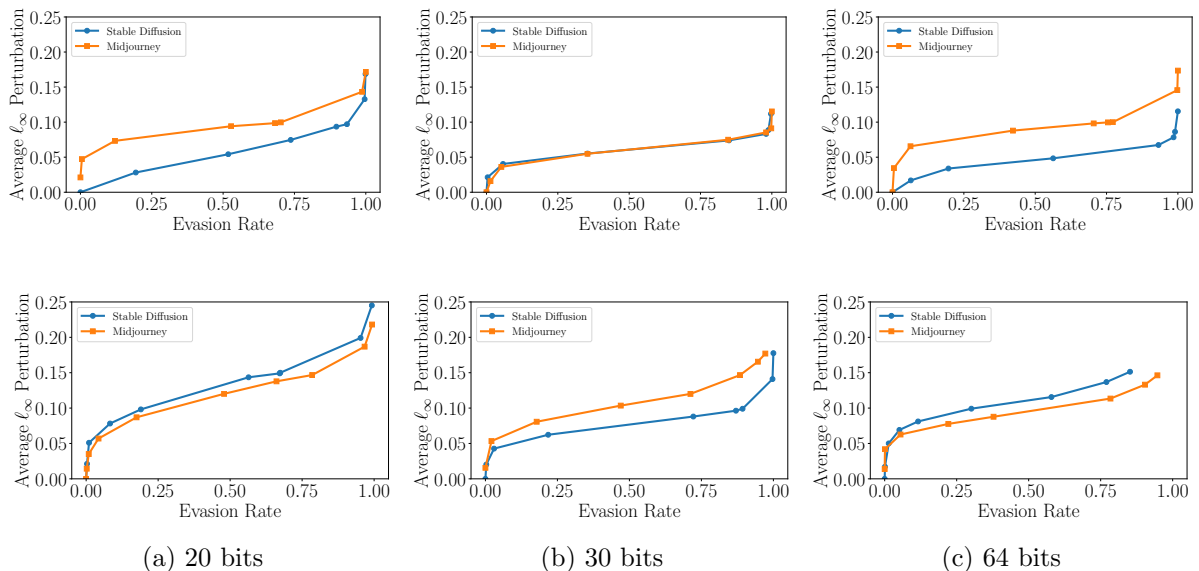


Figure 2: Average perturbation of our transfer attack when the target model uses CNN (*first row*) or ResNet (*second row*) architecture and different watermark lengths (*the three columns*). The surrogate models use CNN architecture and watermark length of 30 bits.

AdvEmb-RN18 [12]. This method uses a ResNet-18 pretrained on ImageNet to generate a feature embedding for a watermarked image. Then it uses PGD to perturb the image such that the embedding of the perturbed image lies far from the one of the watermarked image.

AdvCls-Real&WM [12]. This method involves training a surrogate classifier using both watermarked and non-watermarked images. The watermarked images are generated by the target GenAI and are watermarked by the target watermarking model, and the non-watermarked images are drawn from a distribution different from the one of the images generated by the target GenAI. During attack, PGD is employed to perturb a watermarked image such that it is misclassified by the surrogate classifier as a non-watermarked image.

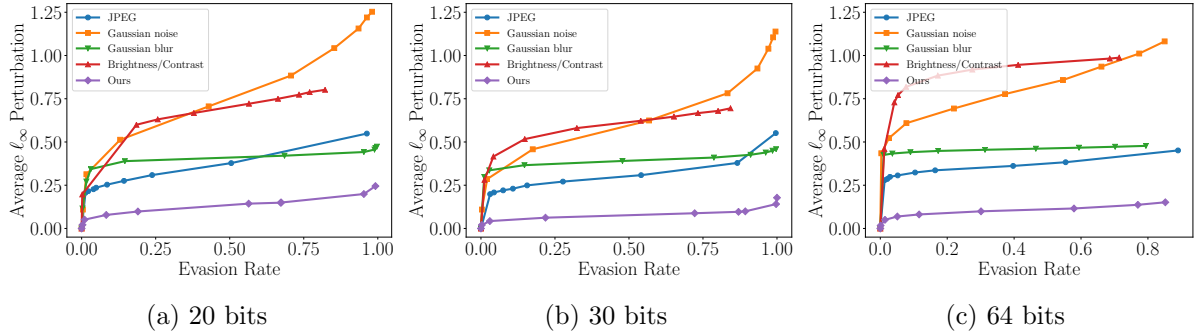


Figure 3: Comparing the average perturbations of our transfer attack and common post-processing methods when they achieve the same evasion rate. The target model uses ResNet architecture and different watermark lengths (*the three columns*). Dataset is Stable Diffusion. Results for Midjourney are shown in Figure 9 in Appendix.

In our experiments, we utilize images generated by DALL-E 2 as the non-watermarked images. More specifically, the training set for the surrogate classifier comprises 8,000 images generated by Stable Diffusion (or Midjourney) and watermarked by the target watermarking model, and 8,000 non-watermarked images generated by DALL-E 2. The surrogate classifier is based on the ResNet-18 architecture.

AdvCls-WM1&WM2 [12]. This method is the same as AdvCls-Real&WM except for the training data used for the surrogate classifier. It assumes that the attacker has access to watermarked images generated by the target watermarking model with two different watermarks. The surrogate classifier is trained to distinguish the watermarked images embedded with one watermark and those embedded with the other watermark. In our experiments, the training set for the surrogate classifier comprises 8,000 images watermarked by the target watermarking model with one watermark, and 8,000 images watermarked by the target watermarking model with the other watermark, where both watermarks are randomly picked.

Evaluation metrics: We mainly use two metrics: *evasion rate* and *average perturbation*. Evasion rate is defined as the proportion of the perturbed images that evade the target watermark-based detector. Average perturbation is the perturbation added to a watermarked image measured by ℓ_∞ -norm averaged across 1,000 watermarked images in the testing set. Following Jiang et al. [11], given that the pixel value range of $[0, 255]$ is normalized to $[-1, 1]$, we adjust the perturbation by dividing it by 2. This adjustment ensures that the perturbation is expressed as a fraction of the full pixel value range $[0, 255]$.

Parameter settings: We use adversarial training to train watermarking models since it enhances robustness. Specifically, for common post-processing methods, we consider the following range of parameters during adversarial training for a target watermarking model: $Q \in [10, 99]$ for JPEG, $\sigma \in [0, 0.1]$ for Gaussian noise, $\sigma \in [0, 2.0]$ for Gaussian blur, and $C \in [1, 3]$ for Brightness/Contrast. For surrogate watermarking models, we adopt a smaller range of parameters for some common post-processing methods during adversarial training to achieve weaker robustness than the target watermarking model as follows: $Q \in [50, 99]$ for JPEG, $\sigma \in [0, 0.1]$ for Gaussian noise, $\sigma \in [0, 1.0]$ for Gaussian blur, and $C \in [1, 3]$ for Brightness/Contrast.

By default, we set $max_iter = 5,000$, $r = 0.25$, $\epsilon = 0.2$, and $\alpha = 0.1$ for our transfer at-

tack. Unless otherwise mentioned, we use Inverse-Decode to select a target watermark for a surrogate decoder, and Ensemble-Optimization to find the perturbation. α is increased when the number of surrogate watermarking models increases in order to satisfy the constraints of our optimization problem within 5,000 iterations. The detailed settings for α for different number of surrogate models are shown in Table 1 in Appendix. Moreover, we use ℓ_2 -distance as the distance metric $l(\cdot, \cdot)$ for two watermarks.

For the detection threshold τ , we set it based on the watermark length of the target watermarking model. Specifically, we set τ to be a value such that the false positive rate of the watermark-based detector is no larger than 10^{-4} when the double-tail detector is employed. Specifically, τ is set to be 0.9, 0.83, and 0.73 for the target watermarking models with watermark lengths of 20 bits, 30 bits, and 64 bits, respectively.

6.2 Experimental Results

Our transfer attack is successful: Figure 1 and Figure 2 respectively show the evasion rate and average perturbation of our transfer attack as the number of surrogate models increases when the target model uses different neural network architectures and watermark lengths on the two datasets. First, we observe that our transfer attack is successful in evading watermark-based detection. The evasion rate is higher than 85% and the average perturbation is no larger than 0.25 when 100 surrogate models are used, no matter what architectures and watermark lengths are used by the target model.

Second, when the target model’s architecture is more complex than the surrogate models’ architecture, our attack requires more surrogate models and larger average perturbation to succeed. For example, our attack uses 40 surrogate models and average perturbation 0.09 to achieve an evasion rate around 100% when the target model is CNN and uses 30-bit watermarks on Stable Diffusion, while our attack uses 60 surrogate models and average perturbation 0.14 to achieve a similar evasion rate when the target model is ResNet and uses 30-bit watermarks. Third, when the target model uses a longer/shorter watermark than the surrogate models, our attack requires more surrogate models and larger average perturbation to succeed. For example, our attack uses 40 surrogate models and average perturbation 0.08 to achieve an evasion rate around 85% when the target model is ResNet and uses 30-bit watermarks, while our attack uses 100 surrogate models and average perturbation 0.15 to achieve a similar evasion rate when the target model uses 64-bit watermarks.

Compare with common post-processing: Figure 3 compares the average perturbations of common post-processing methods and our transfer attack when they achieve the same evasion rates for different target models on the two datasets. Given an evasion rate achieved by our transfer attack using a certain number of surrogate models, we set the parameter of a common post-processing method such that it achieves very close evasion rate. We observe that our transfer attack adds much smaller perturbations than common post-processing methods when achieving the same evasion rate. Note that for some target models, the Brightness/Contrast method can only achieve about 75% evasion rate at most. Thus, the curves for Brightness/Contrast are shorter in the corresponding graphs.

To get a more comprehensive comparison with common post-processing methods, Figure 10 and Figure 11 in Appendix show the comparison results using average perturbation measured by ℓ_2 -norm and average SSIM, respectively. SSIM measures the similarity between a perturbed image and the corresponding watermarked image by considering

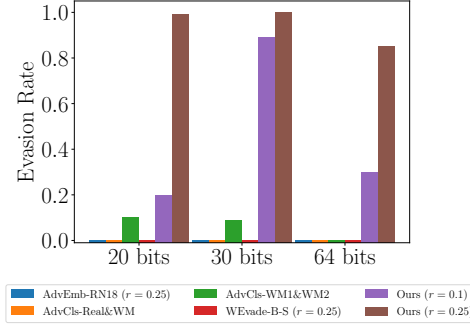


Figure 4: Comparing evasion rates of existing and our transfer attacks when the target model is ResNet and uses watermarks with different lengths. Dataset is Stable Diffusion. Similar results for Midjourney are shown in Figure 12 in Appendix.

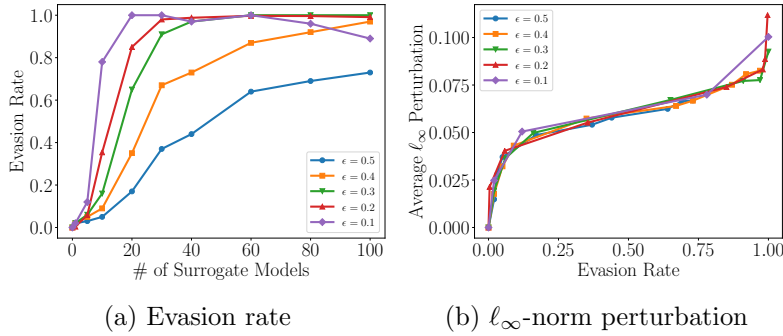


Figure 5: Evasion rate and average ℓ_∞ -norm perturbation of our transfer attack when using different ϵ .

changes in texture, luminance, and contrast. Average SSIM is the SSIM averaged across 1,000 watermarked images and their perturbed versions in the testing set. We still observe that our transfer attack adds much smaller perturbations and thus better maintains the images’ visual quality than common post-processing methods when ℓ_2 -norm or SSIM is used to measure the perturbation.

Compare with existing transfer attacks: Figure 4 compares the evasion rates of existing and our transfer attacks when the target model is ResNet and uses watermarks with different lengths. We note that since AdvCls-Real&Wm and AdvCls-WM1&WM2 can only achieve average perturbation around 0.1 no matter how large the perturbation budget r we set, we add one extra variant of our method with perturbation budget $r = 0.1$ for comparison. For other transfer attacks, the perturbation budget r is set to be 0.25. We observe that our transfer attack is much more effective than other existing transfer attacks. First, we observe that existing transfer attacks achieve almost 0 evasion rates except that AdvCls-WM1&WM2 achieves around 10% evasion rates on the Stable Diffusion dataset when the target model’s watermark length is 20 or 30 bits. This is the reason that existing works concluded that watermarking is robust in the no-box setting. However, our transfer attack achieves much higher evasion rates especially when the perturbation budget is large enough (e.g., $r = 0.25$). We note that the average SSIM of our transfer attack is higher than 0.97 for $r = 0.1$ and higher than 0.92 for $r = 0.25$, which means that the image quality of the perturbed images is maintained well.

Impact of ϵ : Figure 5 shows the evasion rate and average ℓ_∞ -norm perturbation when our transfer attack uses different ϵ on Stable Diffusion dataset, where the target model is

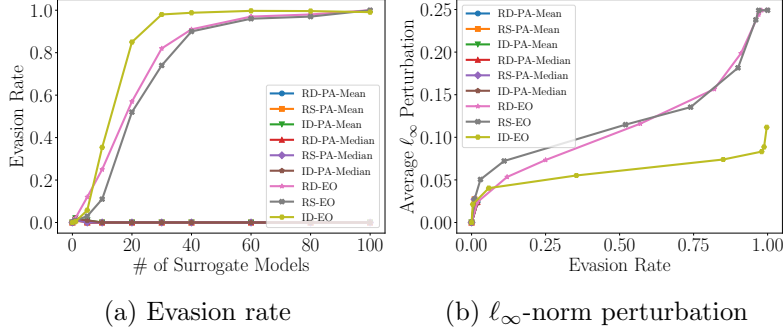


Figure 6: Evasion rates and average ℓ_∞ -norm perturbations of different variants of our transfer attack.

CNN and uses 30-bit watermarks. Figure 13 in Appendix shows the results on average ℓ_2 -norm perturbation and average SSIM. We observe that our attack requires less surrogate models to achieve the same evasion rate when ϵ is smaller. However, when ϵ is too small (e.g., 0.1), the evasion rate first increases and then decreases as the number of surrogate models increases. This is because the bitwise accuracy between the decoded watermark of the perturbed image and the ground-truth watermark becomes too small when ϵ is too small, and thus the perturbed image is still detected as AI-generated by the double-tail detector. Moreover, we observe that, for different ϵ , the average perturbation (measured by ℓ_∞ -norm, ℓ_2 -norm, or SSIM) keeps almost the same when achieving the same evasion rate. This is because the average perturbation and the evasion rate have strong correlations in our attack.

Different variants of our transfer attack: Our attack has two steps, each of which has multiple design choices. We use RD, RS, and ID to respectively denote Random-Different, Random-Same, and Inverse-Decode in the first step; and PA and EO to respectively denote Post-Aggregate and Ensemble-Optimization in the second step. We concatenate the symbols to represent a variant, e.g., RD-PA means using RD and PA as the two steps. Moreover, when PA is used, we further use suffix "Mean" or "Median" to indicate the adopted aggregation rule. For instance, RD-PA-Mean indicates that Mean is used as the aggregation rule.

Figure 6 shows the evasion rate and average ℓ_∞ -norm perturbation when different variants of our transfer attack are used on Stable Diffusion dataset, where the target model is CNN and uses 30-bit watermarks. Figure 13 in Appendix shows the results on average ℓ_2 -norm perturbation and average SSIM. We observe that all the three variants using EO can evade detection successfully while none of the variants using PA can evade detection, which indicates that EO is much more effective at aggregating surrogate decoders than PA. Additionally, within the three variants using EO, RD and RS have similar results for all metrics and are less effective than ID. Specifically, ID-EO achieves 100% evasion rate with less number of surrogate models compared to RD-EO and RS-EO. For the same 100% evasion rate, ID-EO achieves a much lower average ℓ_∞ -norm and ℓ_2 -norm perturbation and a much higher average SSIM than RD-EO and RS-EO.

Theoretical vs. empirical results: Figure 7 shows the empirical average bitwise accuracy between the watermark decoded by the target decoder for a perturbed image and the ground-truth one, and our theoretical upper and lower bounds on Stable Diffusion dataset. The theoretical bounds are estimated as follows: we first measure the unperturbed simi-

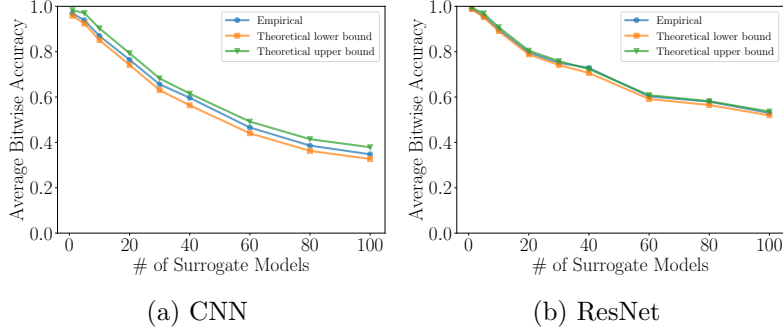


Figure 7: Comparing empirical bitwise accuracy and theoretical bounds of our transfer attack when the target model is (a) CNN and (b) ResNet.

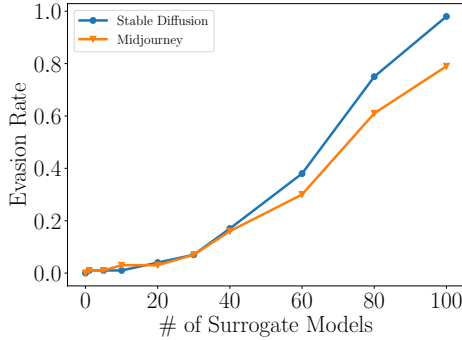


Figure 8: Evasion rate of our transfer attack when the target model is non-learning-based.

larity, transferring similarity, and attacking strength using the 1,000 testing images; then we compute the probability p_j for each j th bit based on Theorem 2, following which we compute the upper and lower bounds of the probability for each bit of the watermark decoded by the target decoder to match with that of the ground-truth watermark; and finally we average these bounds across the bits. We observe that our theoretical upper and lower bounds match well with the empirical bitwise accuracy. Specifically, the empirical results fall within our theoretical bounds except a few cases. Such exception cases happen because the theoretical bounds are estimated using only 1,000 images, resulting in inaccurate estimations.

7 Discussion and Limitations

We focus on transfer attacks to learning-based target watermarking models because learning-based models are more robust than non-learning-based ones. For instance, common post-processing like JPEG compression can already remove watermarks embedded by a non-learning-based model, but learning-based models have good robustness against common post-processing [11]. However, our attack can also be applied to non-learning-based models. For instance, Figure 8 shows the evasion rate of our transfer attack when the target model is the watermarking model used by Stable Diffusion [24] as the number of surrogate models increases on the two datasets, where the surrogate models are the same as those in Section 6. Our results show that our transfer attack can still achieve high evasion rates when the target model is non-learning-based. Compared to when the target model is learning-based, our transfer attack requires more surrogate models to achieve

high (e.g., 100%) evasion rates. This is because non-learning-based watermarking model is substantially different from learning-based, and thus our attack needs more surrogate models to increase diversity and thus enhance transferability.

8 Conclusion and Future Work

In this work, we find that watermark-based detection of AI-generated images is not robust to transfer attacks in the no-box setting. Given a watermarked image, an attacker can remove the watermark by adding a perturbation to it, where the perturbation can be found by ensembling multiple surrogate watermarking models. Our results show that transfer attack based on surrogate watermarking models outperforms those based on surrogate classifiers that treat a watermark-based detector as a conventional classifier. Moreover, leveraging surrogate watermarking models enables us to perform a rigorous analysis on the transferability of our attack. Interesting future work includes extending our transfer attack to text and audio watermarks, as well as designing more robust, especially certifiably robust, watermarks.

References

1. Bi, N., Sun, Q., Huang, D., Yang, Z. & Huang, J. Robust image watermarking based on multiband wavelets and empirical mode decomposition. *IEEE Transactions on Image Processing* (2007).
2. Zhu, J., Kaplan, R., Johnson, J. & Fei-Fei, L. *HiDDeN: Hiding Data with Deep Networks* in *European Conference on Computer Vision* (2018).
3. Tancik, M., Mildenhall, B. & Ng, R. *StegaStamp: Invisible Hyperlinks in Physical Photographs* in *IEEE Conference on Computer Vision and Pattern Recognition* (2020).
4. Zhang, C., Benz, P., Karjauv, A., Sun, G. & Kweon, I. S. *UDH: Universal Deep Hiding for Steganography, Watermarking, and Light Field Messaging* in *Advances in Neural Information Processing Systems* (2020).
5. Al-Haj, A. Combined DWT-DCT digital image watermarking. *Journal of computer science* (2007).
6. Abdelnabi, S. & Fritz, M. *Adversarial watermarking transformer: Towards tracing text provenance with data hiding* in *IEEE Symposium on Security and Privacy* (2021).
7. Kirchenbauer, J. *et al.* *A Watermark for Large Language Models* in *International Conference on Machine Learning* (2023).
8. Saharia, C. *et al.* *Photorealistic text-to-image diffusion models with deep language understanding* in *Advances in Neural Information Processing Systems* (2022).
9. Ramesh, A. *et al.* *Zero-shot text-to-image generation* in *International Conference on Machine Learning* (2021).
10. Rombach, R. *Stable Diffusion watermark decoder* https://github.com/CompVis/stable-diffusion/blob/main/scripts/tests/test_watermark.py. 2022.

11. Jiang, Z., Zhang, J. & Gong, N. Z. *Evading Watermark based Detection of AI-Generated Content in ACM Conference on Computer and Communications Security* (2023).
12. An, B. *et al.* Benchmarking the Robustness of Image Watermarks. *arXiv preprint arXiv:2401.08573* (2024).
13. Madry, A., Makelov, A., Schmidt, L., Tsipras, D. & Vladu, A. *Towards Deep Learning Models Resistant to Adversarial Attacks in International Conference on Learning Representations* (2018).
14. Pereira, S. & Pun, T. Robust template matching for affine resistant image watermarks. *IEEE Transactions on Image Processing* (2000).
15. Kang, X., Huang, J. & Zeng, W. Efficient General Print-Scanning Resilient Data Hiding Based on Uniform Log-Polar Mapping. *IEEE Transactions on Information Forensics and Security* (2010).
16. Pramila, A., Keskinarkaus, A. & Seppänen, T. Increasing the capturing angle in print-cam robust watermarking. *Journal of Systems and Software* (2018).
17. Goodfellow, I. J., Shlens, J. & Szegedy, C. Explaining and harnessing adversarial examples. *arXiv preprint arXiv:1412.6572* (2014).
18. Chen, H., Zhang, Y., Dong, Y. & Zhu, J. Rethinking Model Ensemble in Transfer-based Adversarial Attacks. *arXiv preprint arXiv:2303.09105* (2023).
19. Tramèr, F. *et al.* *Ensemble Adversarial Training: Attacks and Defenses in International Conference on Learning Representations* (2018).
20. Efron, B. & Tibshirani, R. J. *An introduction to the bootstrap* (CRC press, 1994).
21. Wang, Z. J. *et al.* *DiffusionDB: A Large-Scale Prompt Gallery Dataset for Text-to-Image Generative Models in Annual Meeting of the Association for Computational Linguistics* (2023).
22. Turc, I. & Nemade, G. *Midjourney User Prompts & Generated Images (250k)* <https://www.kaggle.com/ds/2349267>. 2022.
23. Images, D. <https://dalle2.gallery>. 2023.
24. Wang, Q. *Invisible watermark* <https://github.com/ShieldMnt/invisible-watermark>. 2020.

Algorithm 1 Find the Perturbation δ

Require: Watermarked image x_w , m surrogate decoders $\{S_i\}_{i=1}^m$, m target watermarks $\{w_i^t\}_{i=1}^m$, distance metric l , perturbation budget r , attack strength threshold ϵ , learning rate α , and maximum number of iterations max_iter .

Ensure: Perturbation δ

- 1: Initialize $\delta \leftarrow 0$
 - 2: **for** $k = 1, 2, \dots, max_iter$ **do**
 - 3: $g \leftarrow \nabla_{\delta} \frac{1}{m} \sum_{i=1}^m l(S_i(x_w + \delta), w_i^t)$
 - 4: $\delta \leftarrow \delta - \alpha \cdot g$
 - 5: **if** $\|\delta\|_{\infty} > r$ **then**
 - 6: $\delta \leftarrow \delta \cdot \frac{r}{\|\delta\|_{\infty}}$
 - 7: **end if**
 - 8: **if** $\frac{1}{m} \sum_{i=1}^m BA(S_i(x_w + \delta), w_i^t) \geq 1 - \epsilon$ **then**
 - 9: Return δ
 - 10: **end if**
 - 11: **end for**
 - 12: Return δ
-

A Proof of Lemma 1

Based on Definition 1, 2, and 3, we have the followings:

$$\begin{aligned} & Pr(T(x_w + \delta)_j = 1 - T(x_w)_j \mid S_i(x_w + \delta)_j = 1 - S_i(x_w)_j) \\ &= Pr(T(x_w + \delta)_j = 1 - T(x_w)_j, T(x_w)_j = S_i(x_w)_j \mid \\ & \quad S_i(x_w + \delta)_j = 1 - S_i(x_w)_j) \\ & \quad + Pr(T(x_w + \delta)_j = 1 - T(x_w)_j, T(x_w)_j = 1 - S_i(x_w)_j \mid \\ & \quad S_i(x_w + \delta)_j = 1 - S_i(x_w)_j) \\ &= Pr(T(x_w + \delta)_j = 1 - T(x_w)_j \mid T(x_w)_j = S_i(x_w)_j, \\ & \quad S_i(x_w + \delta)_j = 1 - S_i(x_w)_j) \\ & \quad \times Pr(T(x_w)_j = S_i(x_w)_j \mid S_i(x_w + \delta)_j = 1 - S_i(x_w)_j) \\ & \quad + Pr(T(x_w + \delta)_j = 1 - T(x_w)_j \mid T(x_w)_j = 1 - S_i(x_w)_j, \\ & \quad S_i(x_w + \delta)_j = 1 - S_i(x_w)_j) \\ & \quad \times Pr(T(x_w)_j = 1 - S_i(x_w)_j \mid S_i(x_w + \delta)_j = 1 - S_i(x_w)_j) \\ &= Pr(T(x_w + \delta)_j = 1 - T(x_w)_j \mid T(x_w)_j = S_i(x_w)_j, \\ & \quad S_i(x_w + \delta)_j = 1 - S_i(x_w)_j) \\ & \quad \times Pr(T(x_w)_j = S_i(x_w)_j \mid S_i(x_w + \delta)_j = 1 - S_i(x_w)_j) \\ & \quad + (1 - Pr(T(x_w + \delta)_j = T(x_w)_j \mid T(x_w)_j = 1 - S_i(x_w)_j, \\ & \quad S_i(x_w + \delta)_j = 1 - S_i(x_w)_j)) \\ & \quad \times (1 - Pr(T(x_w)_j = S_i(x_w)_j \mid S_i(x_w + \delta)_j = 1 - S_i(x_w)_j)) \\ &= Pr(T(x_w + \delta)_j = S_i(x_w + \delta)_j \mid T(x_w)_j = S_i(x_w)_j, \\ & \quad S_i(x_w + \delta)_j = 1 - S_i(x_w)_j) \\ & \quad \times Pr(T(x_w)_j = S_i(x_w)_j \mid S_i(x_w + \delta)_j = 1 - S_i(x_w)_j) \\ & \quad + (1 - Pr(T(x_w + \delta)_j = S_i(x_w + \delta)_j \mid \\ & \quad T(x_w)_j = 1 - S_i(x_w)_j, S_i(x_w + \delta)_j = 1 - S_i(x_w)_j)) \end{aligned}$$

$$\begin{aligned}
& \times (1 - Pr(T(x_w)_j = S_i(x_w)_j \mid S_i(x_w + \delta)_j = 1 - S_i(x_w)_j)) \\
& = a_{ij}k_{ij} + (1 - a'_{ij})(1 - k_{ij}) \\
& = c_{ij}.
\end{aligned}$$

Similarly, we have the following:

$$\begin{aligned}
& Pr(T(x_w + \delta)_j = 1 - T(x_w)_j \mid S_i(x_w + \delta)_j = S_i(x_w)_j) \\
& = Pr(T(x_w + \delta)_j = 1 - T(x_w)_j, T(x_w)_j = S_i(x_w)_j \mid \\
& \quad S_i(x_w + \delta)_j = S_i(x_w)_j) + Pr(T(x_w + \delta)_j = 1 - T(x_w)_j, \\
& \quad T(x_w)_j = 1 - S_i(x_w)_j \mid S_i(x_w + \delta)_j = S_i(x_w)_j) \\
& = Pr(T(x_w + \delta)_j = 1 - T(x_w)_j \mid T(x_w)_j = S_i(x_w)_j, \\
& \quad S_i(x_w + \delta)_j = S_i(x_w)_j) \\
& \quad \times Pr(T(x_w)_j = S_i(x_w)_j \mid S_i(x_w + \delta)_j = S_i(x_w)_j) \\
& \quad + Pr(T(x_w + \delta)_j = 1 - T(x_w)_j \mid T(x_w)_j = 1 - S_i(x_w)_j, \\
& \quad S_i(x_w + \delta)_j = S_i(x_w)_j) \\
& \quad \times Pr(T(x_w)_j = 1 - S_i(x_w)_j \mid S_i(x_w + \delta)_j = S_i(x_w)_j) \\
& = (1 - Pr(T(x_w + \delta)_j = T(x_w)_j \mid T(x_w)_j = S_i(x_w)_j, \\
& \quad S_i(x_w + \delta)_j = S_i(x_w)_j)) \\
& \quad \times Pr(T(x_w)_j = S_i(x_w)_j \mid S_i(x_w + \delta)_j = S_i(x_w)_j) \\
& \quad + Pr(T(x_w + \delta)_j = 1 - T(x_w)_j \mid T(x_w)_j = 1 - S_i(x_w)_j, \\
& \quad S_i(x_w + \delta)_j = S_i(x_w)_j) \\
& \quad \times (1 - Pr(T(x_w)_j = S_i(x_w)_j \mid S_i(x_w + \delta)_j = S_i(x_w)_j)) \\
& = (1 - Pr(T(x_w + \delta)_j = S_i(x_w + \delta)_j \mid T(x_w)_j = S_i(x_w)_j, \\
& \quad S_i(x_w + \delta)_j = S_i(x_w)_j)) \\
& \quad \times Pr(T(x_w)_j = S_i(x_w)_j \mid S_i(x_w + \delta)_j = S_i(x_w)_j) \\
& \quad + Pr(T(x_w + \delta)_j = S_i(x_w + \delta)_j \mid T(x_w)_j = 1 - S_i(x_w)_j, \\
& \quad S_i(x_w + \delta)_j = S_i(x_w)_j) \\
& \quad \times (1 - Pr(T(x_w)_j = S_i(x_w)_j \mid S_i(x_w + \delta)_j = S_i(x_w)_j)) \\
& = (1 - b'_{ij})k'_{ij} + b_{ij}(1 - k'_{ij}) \\
& = c'_{ij}.
\end{aligned}$$

B Proof of Theorem 1

Based on Lemma 1 and Definition 4, we have the following:

$$\begin{aligned}
& Pr(T(x_w + \delta)_j = 1 - T(x_w)_j) \\
& = Pr(T(x_w + \delta)_j = 1 - T(x_w)_j, S_i(x_w + \delta) = S_i(x_w)) \\
& \quad + Pr(T(x_w + \delta)_j = 1 - T(x_w)_j, S_i(x_w + \delta) = 1 - S_i(x_w)) \\
& = Pr(T(x_w + \delta)_j = 1 - T(x_w)_j \mid S_i(x_w + \delta) = S_i(x_w)) \\
& \quad \times Pr(S_i(x_w + \delta) = S_i(x_w)) \\
& \quad + Pr(T(x_w + \delta)_j = 1 - T(x_w)_j \mid S_i(x_w + \delta) = 1 - S_i(x_w))
\end{aligned}$$

$$\begin{aligned}
& \times \Pr(S_i(x_w + \delta) = 1 - S_i(x_w)) \\
& = c'_{ij}(1 - q_{ij}) + c_{ij}q_{ij} \\
& = e_j.
\end{aligned}$$

C Proof of Lemma 2

$$\begin{aligned}
& \Pr(S_i(x_w + \delta)_j = 1 - S_i(x_w)_j \mid T(x_w + \delta)_j = 1 - T(x_w)_j) \\
& = \frac{\Pr(S_i(x_w + \delta)_j = 1 - S_i(x_w)_j, T(x_w + \delta)_j = 1 - T(x_w)_j)}{\Pr(T(x_w + \delta)_j = 1 - T(x_w)_j)} \\
& = \Pr(T(x_w + \delta)_j = 1 - T(x_w)_j \mid S_i(x_w + \delta)_j = 1 - S_i(x_w)_j) \\
& \quad \times \frac{\Pr(S_i(x_w + \delta)_j = 1 - S_i(x_w)_j)}{\Pr(T(x_w + \delta)_j = 1 - T(x_w)_j)}.
\end{aligned}$$

Based on Lemma 1 and Theorem 1, we have the following:

$$\begin{aligned}
& \Pr(T(x_w + \delta)_j = 1 - T(x_w)_j \mid S_i(x_w + \delta)_j = 1 - S_i(x_w)_j) \\
& \quad \times \frac{\Pr(S_i(x_w + \delta)_j = 1 - S_i(x_w)_j)}{\Pr(T(x_w + \delta)_j = 1 - T(x_w)_j)} \\
& = \frac{c_{ij}q_{ij}}{c_{ij}q_{ij} + c'_{ij}(1 - q_{ij})}.
\end{aligned}$$

D Proof of Theorem 2

$$\begin{aligned}
& \Pr(T(x_w + \delta)_j = 1 - T(x_w)_j \mid S_1(x_w + \delta)_j, \dots, S_m(x_w + \delta)_j) \\
& = \Pr(S_1(x_w + \delta)_j, \dots, S_m(x_w + \delta)_j \mid \\
& \quad T(x_w + \delta)_j = 1 - T(x_w)_j) \\
& \quad \times \frac{\Pr(T(x_w + \delta)_j = 1 - T(x_w)_j)}{\Pr(S_1(x_w + \delta)_j, \dots, S_m(x_w + \delta)_j)}.
\end{aligned}$$

Based on Assumption 2 and 3, we have the following:

$$\begin{aligned}
& \Pr(S_1(x_w + \delta)_j, \dots, S_m(x_w + \delta)_j \mid T(x_w + \delta)_j = 1 - T(x_w)_j) \\
& \quad \times \frac{\Pr(T(x_w + \delta)_j = 1 - T(x_w)_j)}{\Pr(S_1(x_w + \delta)_j, \dots, S_m(x_w + \delta)_j)} \\
& = \Pr(S_1(x_w + \delta)_j \mid T(x_w + \delta)_j = 1 - T(x_w)_j) \\
& \quad \cdots \Pr(S_m(x_w + \delta)_j \mid T(x_w + \delta)_j = 1 - T(x_w)_j) \\
& \quad \times \frac{\Pr(T(x_w + \delta)_j = 1 - T(x_w)_j)}{\Pr(S_1(x_w + \delta)_j) \cdots \Pr(S_m(x_w + \delta)_j)}. \tag{16}
\end{aligned}$$

Given that $M_{j1} = \{i \mid S_i(x_w + \delta)_j = 1 - S_i(x_w)_j\}$, we have the following according to Lemma 2:

$$\Pr(S_i(x_w + \delta)_j \mid T(x_w + \delta)_j = 1 - T(x_w)_j)$$

$$\begin{aligned}
&= Pr(S_i(x_w + \delta)_j = 1 - S_i(x_w) \mid T(x_w + \delta)_j = 1 - T(x_w)_j) \\
&= \frac{c_{ij}q_{ij}}{c_{ij}q_{ij} + c'_{ij}(1 - q_{ij})}, \forall i \in M_{j1}.
\end{aligned} \tag{17}$$

Given that $M_{j2} = \{i \mid S_i(x_w + \delta)_j = S_i(x_w)_j\}$, we have:

$$\begin{aligned}
&Pr(S_i(x_w + \delta)_j \mid T(x_w + \delta)_j = 1 - T(x_w)_j) \\
&= 1 - Pr(S_i(x_w + \delta)_j = 1 - S_i(x_w) \mid \\
&\quad T(x_w + \delta)_j = 1 - T(x_w)_j) \\
&= 1 - \frac{c_{ij}q_{ij}}{c_{ij}q_{ij} + c'_{ij}(1 - q_{ij})} \\
&= \frac{c'_{ij}(1 - q_{ij})}{c_{ij}q_{ij} + c'_{ij}(1 - q_{ij})}, \forall i \in M_{j2}.
\end{aligned} \tag{18}$$

Then Equation 16 can be reformulated as follows:

$$\begin{aligned}
&Pr(S_1(x_w + \delta)_j \mid T(x_w + \delta)_j = 1 - T(x_w)_j) \\
&\quad \cdots Pr(S_m(x_w + \delta)_j \mid T(x_w + \delta)_j = 1 - T(x_w)_j) \\
&\quad \times \frac{Pr(T(x_w + \delta)_j = 1 - T(x_w)_j)}{Pr(S_1(x_w + \delta)_j) \cdots Pr(S_m(x_w + \delta)_j)} \\
&= Pr(T(x_w + \delta)_j = 1 - T(x_w)_j) \\
&\quad \prod_{i \in M_{j1}} \frac{Pr(S_i(x_w + \delta)_j \mid T(x_w + \delta)_j = 1 - T(x_w)_j)}{Pr(S_i(x_w + \delta)_j)} \\
&\quad \prod_{i \in M_{j2}} \frac{Pr(S_i(x_w + \delta)_j \mid T(x_w + \delta)_j = 1 - T(x_w)_j)}{Pr(S_i(x_w + \delta)_j)}.
\end{aligned}$$

Then, based on Definition 4, Theorem 1, Equation 17, and Equation 18, we have the following:

$$\begin{aligned}
&Pr(T(x_w + \delta)_j = 1 - T(x_w)_j) \\
&\quad \prod_{i \in M_{j1}} \frac{Pr(S_i(x_w + \delta)_j \mid T(x_w + \delta)_j = 1 - T(x_w)_j)}{Pr(S_i(x_w + \delta)_j)} \\
&\quad \prod_{i \in M_{j2}} \frac{Pr(S_i(x_w + \delta)_j \mid T(x_w + \delta)_j = 1 - T(x_w)_j)}{Pr(S_i(x_w + \delta)_j)} \\
&= e_j \prod_{i \in M_{j1}} \frac{c_{ij}q_{ij}}{c_{ij}q_{ij}^2 + c'_{ij}(1 - q_{ij})q_{ij}} \\
&\quad \prod_{i \in M_{j2}} \frac{c'_{ij}(1 - q_{ij})}{c_{ij}q_{ij}(1 - q_{ij}) + c'_{ij}(1 - q_{ij})^2} \\
&= \min(e_j \prod_{i \in M_{j1}} \frac{c_{ij}}{c_{ij}q_{ij} + c'_{ij}(1 - q_{ij})} \\
&\quad \prod_{i \in M_{j2}} \frac{c'_{ij}}{c_{ij}q_{ij} + c'_{ij}(1 - q_{ij})}, 1) \\
&= p_j.
\end{aligned}$$

E Proof of Theorem 3

The conditional expectation of $|T(x_w + \delta)_j - T(x_w)_j|$ can be represented as:

$$\begin{aligned}
& E(|T(x_w + \delta)_j - T(x_w)_j| \mid S_1(x_w + \delta)_j, \dots, S_m(x_w + \delta)_j) \\
&= 0 \times Pr(T(x_w + \delta)_j = T(x_w)_j \mid \\
&\quad S_1(x_w + \delta)_j, \dots, S_m(x_w + \delta)_j) \\
&\quad + 1 \times Pr(T(x_w + \delta)_j = 1 - T(x_w)_j \mid \\
&\quad S_1(x_w + \delta)_j, \dots, S_m(x_w + \delta)_j) \\
&= Pr(T(x_w + \delta)_j = 1 - T(x_w)_j \mid \\
&\quad S_1(x_w + \delta)_j, \dots, S_m(x_w + \delta)_j).
\end{aligned}$$

According to Theorem 2, we have:

$$\begin{aligned}
& Pr(T(x_w + \delta)_j = 1 - T(x_w)_j \mid S_1(x_w + \delta)_j, \dots, S_m(x_w + \delta)_j) \\
&= p_j.
\end{aligned}$$

According to Assumption 3, the conditional expectation of $|T(x_w)_j - w_j|$ can be represented as:

$$\begin{aligned}
& E(|T(x_w)_j - w_j| \mid S_1(x_w + \delta)_j, \dots, S_m(x_w + \delta)_j) \\
&= 0 \times Pr(T(x_w)_j = w_j \mid S_1(x_w + \delta)_j, \dots, S_m(x_w + \delta)_j) \\
&\quad + 1 \times Pr(T(x_w)_j = 1 - w_j \mid \\
&\quad S_1(x_w + \delta)_j, \dots, S_m(x_w + \delta)_j) \\
&= Pr(T(x_w)_j = 1 - w_j \mid S_1(x_w + \delta)_j, \dots, S_m(x_w + \delta)_j) \\
&= \frac{Pr(T(x_w)_j = 1 - w_j, S_1(x_w + \delta)_j, \dots, S_m(x_w + \delta)_j)}{Pr(S_1(x_w + \delta)_j, \dots, S_m(x_w + \delta)_j)} \\
&= \frac{Pr(S_1(x_w + \delta)_j, \dots, S_m(x_w + \delta)_j \mid T(x_w)_j = 1 - w_j)}{Pr(S_1(x_w + \delta)_j, \dots, S_m(x_w + \delta)_j)} \\
&\quad \times Pr(T(x_w)_j = 1 - w_j) \\
&= \frac{Pr(S_1(x_w + \delta)_j \mid T(x_w)_j = 1 - w_j)}{Pr(S_1(x_w + \delta)_j)} \\
&\quad \dots \frac{Pr(S_m(x_w + \delta)_j \mid T(x_w)_j = 1 - w_j)}{Pr(S_m(x_w + \delta)_j)} \\
&\quad \times Pr(T(x_w)_j = 1 - w_j).
\end{aligned}$$

Since the flipping behavior of surrogate models is irrelevant to Definition 5, then we have the following:

$$\begin{aligned}
& E(|T(x_w)_j - w_j| \mid S_1(x_w + \delta)_j, \dots, S_m(x_w + \delta)_j) \\
&= Pr(T(x_w)_j = 1 - w_j).
\end{aligned}$$

Based on Definition 5, we have:

$$E(|T(x_w)_j - w_j| \mid S_1(x_w + \delta)_j, \dots, S_m(x_w + \delta)_j)$$

Table 1: The detailed settings of α for different number of surrogate models.

# of Surrogate Models	1	5	10	20	30	40	60	80	100
α		0.1			1		2		4

$$= 1 - \beta_j.$$

Furthermore, the conditional expectation of $|T(x_w + \delta)_j - w_j|$ can be represented as:

$$\begin{aligned}
& E(|T(x_w + \delta)_j - w_j| \mid S_1(x_w + \delta)_j, \dots, S_m(x_w + \delta)_j) \\
&= 0 \times Pr(T(x_w + \delta)_j = w_j \mid S_1(x_w + \delta)_j, \dots, S_m(x_w + \delta)_j) \\
&\quad + 1 \times Pr(T(x_w + \delta)_j = 1 - w_j \mid \\
&\quad\quad S_1(x_w + \delta)_j, \dots, S_m(x_w + \delta)_j) \\
&= Pr(T(x_w + \delta)_j = 1 - w_j \mid S_1(x_w + \delta)_j, \dots, S_m(x_w + \delta)_j). \tag{19}
\end{aligned}$$

Based on the triangle inequality, we have the following:

$$\begin{aligned}
& E(|T(x_w + \delta)_j - w_j| \mid S_1(x_w + \delta)_j, \dots, S_m(x_w + \delta)_j) \\
&\leq \min(E(|T(x_w + \delta)_j - T(x_w)_j| + |T(x_w)_j - w_j| \mid \\
&\quad S_1(x_w + \delta)_j, \dots, S_m(x_w + \delta)_j), 1) \\
&= \min(1 - \beta_j + p_j, 1),
\end{aligned}$$

and the following:

$$\begin{aligned}
& E(|T(x_w + \delta)_j - w_j| \mid S_1(x_w + \delta)_j, \dots, S_m(x_w + \delta)_j) \\
&\geq E(|T(x_w + \delta)_j - T(x_w)_j| - |T(x_w)_j - w_j| \mid \\
&\quad S_1(x_w + \delta)_j, \dots, S_m(x_w + \delta)_j) \\
&= |p_j + \beta_j - 1|.
\end{aligned}$$

Therefore, based on Equation 19, we have the following:

$$\begin{aligned}
& Pr(T(x_w + \delta)_j = w_j \mid S_1(x_w + \delta)_j, \dots, S_m(x_w + \delta)_j) \\
&= 1 - Pr(T(x_w + \delta)_j = 1 - w_j \mid \\
&\quad S_1(x_w + \delta)_j, \dots, S_m(x_w + \delta)_j) \\
&\geq 1 - \min(1 - \beta_j + p_j, 1) \\
&= \max(\beta_j - p_j, 0),
\end{aligned}$$

and the following:

$$\begin{aligned}
& Pr(T(x_w + \delta)_j = w_j \mid S_1(x_w + \delta)_j, \dots, S_m(x_w + \delta)_j) \\
&\leq 1 - |p_j + \beta_j - 1|.
\end{aligned}$$

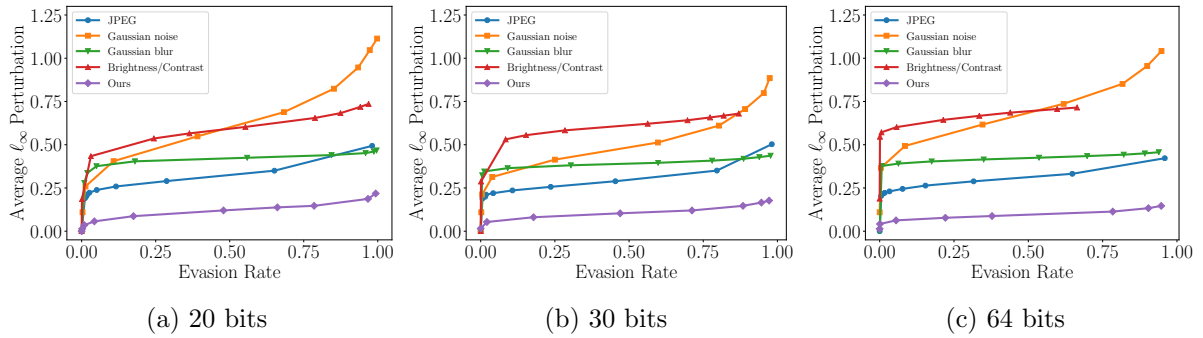


Figure 9: Comparing the average perturbations of our transfer attack and common post-processing methods when they achieve the same evasion rate. The target model uses ResNet architecture and different watermark lengths (*the three columns*). Dataset is Midjourney.

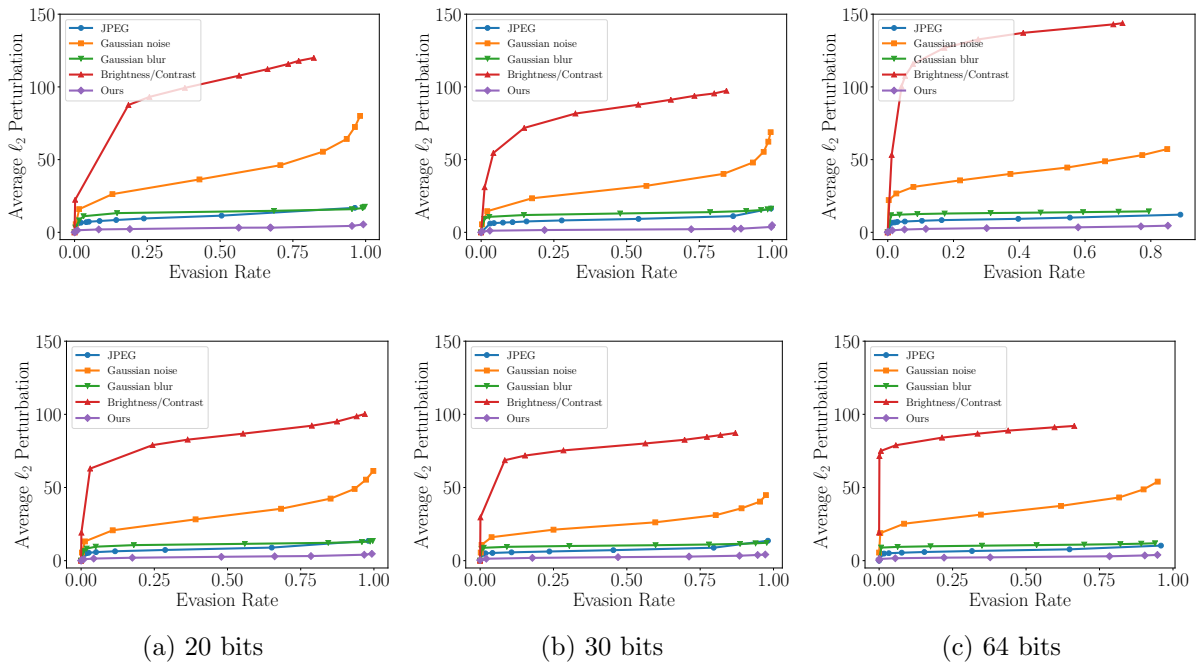


Figure 10: Comparing the average ℓ_2 -norm perturbations of our transfer attack and common post-processing methods when they achieve the same evasion rate. The target model uses ResNet architecture and different watermark lengths (*the three columns*). *First row*: Stable Diffusion. *Second row*: Midjourney.

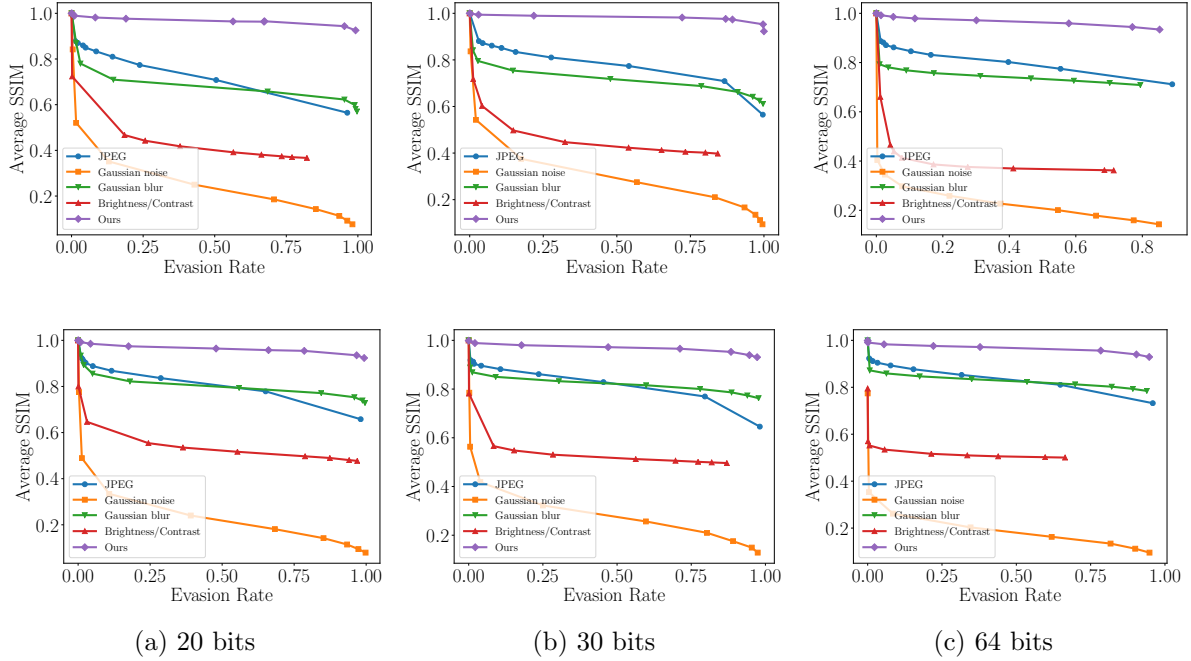


Figure 11: Comparing the average SSIM of our transfer attack and common post-processing methods when they achieve the same evasion rate. The target model uses ResNet architecture and different watermark lengths (*the three columns*). *First row*: Stable Diffusion. *Second row*: Midjourney.

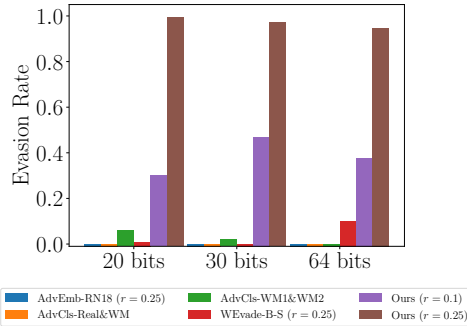


Figure 12: Comparing the evasion rates of existing and our transfer attacks when the target model is ResNet and uses watermarks with different lengths. Dataset is Midjourney.

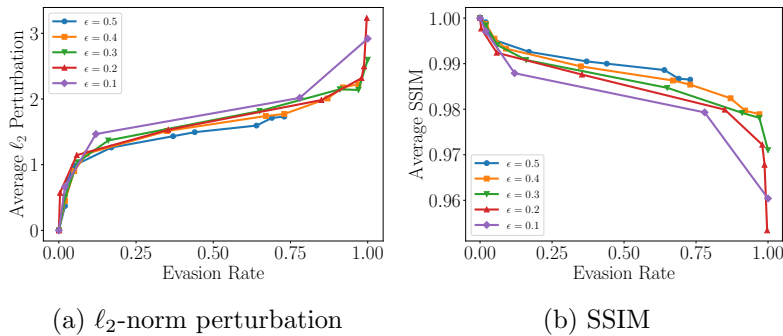
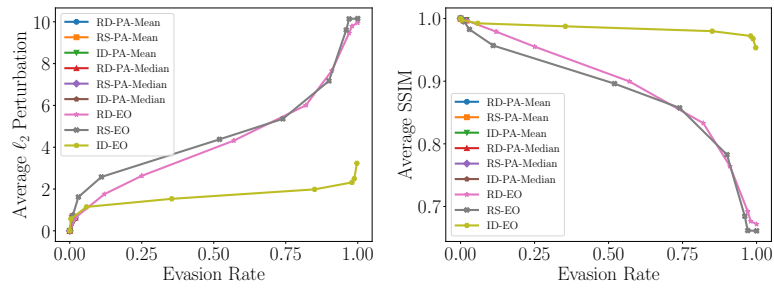


Figure 13: Average ℓ_2 -norm perturbations and average SSIM of our transfer attack with different ϵ . The target model uses CNN architecture and watermark length of 30 bits.



(a) ℓ_2 -norm perturbation

(b) SSIM

Figure 14: Average ℓ_2 -norm perturbations and average SSIM of different variants of our transfer attack. The target model uses CNN architecture and watermark length of 30 bits.